Ecotoxicology and Environmental Safety 256 (2023) 114863

Contents lists available at ScienceDirect

Ecotoxicology and Environmental Safety

journal homepage: www.elsevier.com/locate/ecoenv

Aluminum hydroxide exposure induces neurodevelopmental impairment in hESC-derived cerebral organoids

Liuyongwei Wang [a], Linqiang Mei [b,c], Zhenle Zang [a], Yun Cai [a], Peiyan Jiang [a], Lianyu Zhou [a], Zhulin Du [a], Ling Yang [a], Zhanjun Gu [b,c], Tianyao Liu [a,*], Xiaotang Fan [a,*]

[a] Department of Military Cognitive Psychology, School of Psychology, Third Military Medical University (Army Medical University), Chongqing 400038, China
[b] CAS Key Laboratory for Biomedical Effects of Nanomaterials and Nanosafety and CAS Center for Excellence in Nanoscience, Institute of High Energy Physics and National Center for Nanoscience and Technology, Chinese Academy of Sciences, Beijing 100049, China
[c] College of Materials Science and Optoelectronic Technology, University of Chinese Academy of Sciences, Beijing 100049, China

ARTICLE INFO

Edited by Dr. Yong Liang

Keywords:
Aluminum hydroxide
Cerebral organoids
Neurotoxicity
Neural progenitor cells
Hippo signaling pathway
Human embryonic stem cells

ABSTRACT

Aluminum (Al) has been classified as a cumulative environmental pollutant that endangers human health. There is increasing evidence to suggest the toxic effects of Al, but the specific action on human brain development remains unclear. Al hydroxide ($Al(OH)_3$), the most common vaccine adjuvant, is the major source of Al and poses risks to the environment and early childhood neurodevelopment. In this study, we explored the neurotoxic effect of 5 μg/ml or 25 μg/ml $Al(OH)_3$ for six days on neurogenesis by utilizing human cerebral organoids from human embryonic stem cells (hESCs). We found that early $Al(OH)_3$ exposure in organoids caused a reduction in the size, deficits in basal neural progenitor cell (NPC) proliferation, and premature neuron differentiation in a time and dose-dependent manner. Transcriptomes analysis revealed a markedly altered Hippo-YAP1 signaling pathway in $Al(OH)_3$ exposed cerebral organoid, uncovering a novel mechanism for $Al(OH)_3$-induced detrimental to neurogenesis during human cortical development. We further identified that $Al(OH)_3$ exposure at day 90 mainly decreased the production of outer radial glia-like cells(oRGs) but promoted NPC toward astrocyte differentiation. Taken together, we established a tractable experimental model to facilitate a better understanding of the impact and mechanism of $Al(OH)_3$ exposure on human brain development.

1. Introduction

Aluminum (Al) is one of the most abundant metals on earth and is widely used in medicine, pharmacy, food technology, and cosmetics (Alasfar and Isaifan, 2021; Exley, 2003). Al exposure occurs mainly through the environment, occupational, and dietary factors for humans (Exley, 2013), such as deodorants, cosmetics, dyes, processed foods, antacids, medicinal pills, drinking water, flame retardant, anti-acid medication, and vaccine adjuvant (Lindblad, 2004; Walton, 2007; Yokel et al., 2008). Previous studies have shown that Al can accumulate in specific brain regions for a long time (Couette et al., 2009). There is a lot of evidence implicating that Al leads to neurotoxicity in the central nervous system (CNS) (Shaw and Tomljenovic, 2013), including deficits in neurotransmission and synaptic activity (Zhang, 2018), disruption of the blood-brain barrier (Wang, 2018), brain inflammation (Bondy, 2010), impaired brain-specific gene transcription (Pogue and Lukiw, 2016), and amyloidosis (Mold et al., 2020). Furthermore, analysis of human biological samples revealed that mothers and their newborns had almost identical blood Al levels (Aziz et al., 2017), and preterm infants suffering from prolonged intravenous feeding with solutions

Abbreviations: Al, Aluminum; $Al(OH)_3$, Aluminum hydroxide; hESCs, human embryonic stem cells; NPCs, neural progenitor cells; oRGs, outer radial glia-like cells; CNS, central nervous system; MMF, Macrophagic Myofasciitis; ASIA, Autoimmune/inflammatory syndrome; ASD, autism spectrum disorder; hiPSCs, human induced pluripotent stem cells; RNA-seq, RNA sequencing; SEM, Scanning electron microscope; PFA, paraformaldehyde; PBS, phosphate buffered saline; OCT, optimal cutting temperature compound; CCK8, Cell Counting Kit-8; TUNEL, Terminal Deoxynucleotidyl Transferase mediated dUTP Nick-End Labeling; DMSO, dimethyl sulfoxide; ICP-MS, Inductively coupled plasma-mass spectrometry analyses; VZ, ventricular zone; CP, cortical plate; oSVZ, outer subventricular zone; SVZ, subventricular zone aRGs, apical radial glia cells; RGCs, radial glia cells; EdU, 5-ethynyl-2 -deoxyuridine; qPCR, quantitative reverse transcription PCR; DEGs, differentially expressed genes; GO, Gene Ontology; KEGG, Kyoto Encyclopedia of Genes and Genomes; BP, biological process.

* Corresponding authors.
E-mail addresses: squall277@163.com (T. Liu), fanxiaotang2005@163.com (X. Fan).

https://doi.org/10.1016/j.ecoenv.2023.114863
Received 9 December 2022; Received in revised form 25 March 2023; Accepted 30 March 2023
Available online 1 April 2023
0147-6513/© 2023 The Author(s). Published by Elsevier Inc. This is an open access article under the CC BY-NC-ND license (http://creativecommons.org/licenses/by-nc-nd/4.0/).

contaminated with Al have impaired brain development (Bishop et al., 1997).

Of note, the source of Al at a very young age is vaccine adjuvant aiming to stimulate an immune response (Lindblad, 2004). Although a single vaccine may contain only a small amount of Al (usually less than 0.5 mg of the adjuvant compound, not elemental Al), multiple vaccines with Al adjuvants can contribute significantly to the overall Al burden on the body. Pediatric vaccine schedules in many countries indicate children will receive 23–32 vaccines, many with Al adjuvants. The administration of 20 or more vaccines containing 0.5 mg of the Al compound as adjuvants would add up to an extra 10 mg of Al compound to the body burden, equivalent to a normal dietary intake of Al of over 4000 mg/day (Shaw, 2018). There are various kinds of Al adjuvant preparations, but Al hydroxide ($Al(OH)_3$) is the more widely used adjuvant (Brunner et al., 2010). Previous studies have reported that the long-term persistence of $Al(OH)_3$ in innate immune cells leads to specific lesions at immune sites, called Macrophagic myofasciitis (MMF) (Gherardi et al., 2015), which may be detected up to >12 years after the last vaccine injection in patients with a clinical condition now designated as Autoimmune/inflammatory syndrome(ASIA) (Lujan et al., 2013) induced by adjuvants. Experimental studies also have shown a range of behavioral abnormalities (Sheth et al., 2018) and associated motor neuron death in young mice following postnatal exposure to vaccine adjuvants at 100μgAl/kg (Petrik et al., 2007). Similarly, neuroinflammatory/degenerative syndromes have been reported in sheep following repeated injections of Al-containing vaccines (Lujan et al., 2013). It has been indicated the correlation between Al in vaccines and the rising prevalence of autism spectrum disorder (ASD) (Angrand et al., 2022; Boretti, 2021; Tomljenovic and Shaw, 2011). The adverse effects of Al adjuvants on the developing human CNS need to be concerned (Principi and Esposito, 2018), in view of that children are regularly exposed to significant amounts of Al from vaccines. However, due to strict ethical restrictions and practical issues, the harmful effects of Al $(OH)_3$ exposure on human nervous system development are not well understood.

Cerebral organoid, an ideal complex and multicellular organotypic in vitro model which is derived from human embryonic stem cells (hESCs) or human induced pluripotent stem cells (hiPSCs), recapitulates most of the molecular, cellular, and anatomical features of human early brain development (Lancaster and Knoblich, 2014). Recent advanced technologies for culturing cerebral organoids emerged as a promising in vitro experimental model for investigating human brain developmental diseases and neurotoxicity induced by a variety of drugs or environmental pollutants (Fan et al., 2022; Li et al., 2022). More importantly, the formation of cortical-like structures in cultured cerebral organoids recapitulates the development of the human cortex by generating progenitor layers similar to the outer subventricular zone (oSVZ), including the outer radial glia (oRG) cells (Li et al., 2022). Here the cerebral organoids model derived from hESCs was used to mimic human early brain development and to explore the potential adverse effects of Al $(OH)_3$ on brain development in a dynamic neurodevelopmental context.

2. Materials and methods

2.1. Chemicals

$Al(OH)_3$ solid particle in size from 3 to 10 μm was kindly provided by the CAS Key Laboratory for Biomedical Effects of Nanomaterials and Nanosafety and CAS Center for Excellence in Nanoscience. Scanning electron microscope (SEM) images of $Al(OH)_3$ were shown in Fig. S1. Al $(OH)_3$ was dispersed in dimethyl sulfoxide (DMSO) at a stock concentration of 100 mg/ml and stored in dark at 4 °C. The solutions were sonicated for 10 min and mixed completely before treatment.

2.2. hESC culturing and generation of cerebral organoid

The hESC line (H9) was kindly provided by the Stem Cell Bank, Chinese Academy of Sciences (CAS). The cell line was cultured without feeders using Essential 8™ Culture Medium (A1517001, Gibco) with 10 μm Y-27632 rock inhibition. The induction of cerebral organoids followed Lancaster's protocol (Giandomenico et al., 2021; Lancaster and Knoblich, 2014). In brief, when hESCs colonies grown in a 6-well plate reached about 70%–80% confluency, they were digested into single-cell suspensions with Tryple (12604013, Gibco) and added into ultra-low attachment 96-well plates with 9000 cells per well to generate embryoid bodies (EBs) at day 0. EBs were formed with smooth edges and cultured in the 96-well plate for six days, then were transferred to neural induction media containing N2 for another six days. On day 12, the EBs with smooth edges were embedded in Matrigel droplets to promote the expansion of the neuroepithelial buds for four days with a differentiation medium. On day 16, cerebral organoids were transferred on an orbital shaker (17504044, Invitrogen, USA) with a maturation medium. On day 20, most of the Matrigel around each organoid was carefully removed using two syringe needles and maintained in medium culture.

2.3. $Al(OH)_3$ exposure

The hESC cells were exposed to Essential 8 culture media containing a series of concentrations of $Al(OH)_3$ ranging from 0, 0.1, 0.5, 1,2, 3, 4, 5, 25, 50, to 100 μg/ml (0 μg/ml as the control group) for 24 h and 48 h, respectively. Cerebral organoids at days 22 or 90 were treated with Al $(OH)_3$ for six days to evaluate their neurotoxicity. On day 22, the cerebral organoids exposed to mature culture media containing $Al(OH)_3$ at a concentration of 0, 5, 25 μg/ml for six days were used for general investigation and collected on days 28 and 56. Outer radial glia (oRG) and astrocytes were analyzed in day 96 organoids following 25 μg/ml Al $(OH)_3$ exposure for six days. The organoids in control groups were cultured in a maturation medium.

2.4. Immunofluorescence staining

The hESC cells were fixed with 4% paraformaldehyde (PFA) at room temperature for 20 min. The cerebral organoids were fixed with 4% PFA overnight at 4 °C and then transferred to 30% sucrose solution at 4 °C until the samples were completely dehydrated. After embedding in optimal cutting temperature compound (OCT) , the cerebral organoids were cut into 20-μm-thick sections and placed on adhesive slides at −20 °C. For immunofluorescence staining, sections were washed in PBS to clear the OCT and treated with 0.03% Triton-x for 30 min at 37 °C. Sections were incubated with the primary antibodies at 37 °C for 2 h and then at room temperature overnight, then were washed thoroughly and incubated with secondary antibodies at 37 °C for 2 h. After counterstaining with DAPI, the sections were examined and photographed using the ZEISS microscope. The antibodies used in this study were listed in table S1.

2.5. Real-time PCR

The total RNA was extracted with Trizol (Gibco) and reverse transcribed into cDNA with RevertAid MM (Thermo Scientific, M1631) following the manufacturer's instruction. The qPCR was conducted by SYBR Green Master kit (Gibco, 4309155) using the primers in Table S2. All data were normalized to GAPDH to analyze the relative gene expression by the $2^{-\Delta\Delta CT}$ method. Data from three parallel groups were presented as mean±SEM.

2.6. Cell viability assays

Cell Counting Kit-8 (Dojindo, CK04) assays were accessed the viability of hESC cells after $Al(OH)_3$ treatment(5 μg/ml, 25 μg/ml, 50

μg/ml, 100 μg/ml). Approximately 5 × 10^4 single cells in 100 μl Essential 8^{TM} medium were seeded in 96-well plates for 24 h, then different concentrations of $Al(OH)_3$ were added to plates for another 24 h. Subsequently, 10 μl CCK8 working solution was added into each well and incubated in the dark at 37 °C for 2–4 h. The absorbance value was determined with a microplate reader at 450 nm. Data of parallel groups were presented as mean±SEM.

2.7. TUNEL assays (terminal deoxynucleotidyl transferase mediated dUTP nick-end labeling)

Apoptosis of hESCs and cerebral organoids in three parallel groups after treatment was detected using the TUNEL assay kit. Briefly, the TUNEL reaction mixture preparation: end-labeling enzyme and labeling liquid were mixed at a ratio of 1:9 and then diluted with 0.1 M PBS, and sections were incubated with the reaction resolution at 37 °C for 30 min in the dark, followed by immuno-staining.

2.8. Western blot

The human cerebral organoids samples were collected and processed as previously described(Liu et al., 2019). The protein (30 μg) was loaded on 10% SDS-PAGE and separated by electrophoresis, and then transferred to the PVDF membrane (Bio-Rad). The membranes were incubated with diluted antibodies (listed in table S1). The immunoreactive bands were visualized by chemiluminescent HRP substrate (Millipore). The intensities of the immunoreactive bands were determined with Image Lab (Bio-Rad Laboratories, United States). The protein level was analyzed using the semi-quantitative method by comparing it with GAPDH.

2.9. RNA-sequencing

The cerebral organoids in the $Al(OH)_3$ treatment group with different concentrations were collected on day 28 for the mRNA sequencing assay. Total RNA was isolated using a Trizol reagent kit (Gibco, 15596018) based on the manual instructions. Subsequently, The Agilent 2100 Bioanalyzer detected RNA concentration, RIN value, 28 S/18 S, and fragment size to determine RNA integrity. To generate sequencing libraries, the following steps were followed. Firstly, We used magnetic beads containing Oligo(dT) to enrich mRNA. A fragmentation buffer was added to break the mRNA into short fragments. The first strand of cDNA was synthesized from mRNA using random hexamers, followed by the buffer, dNTPs, and RNaseH. A second strand of cDNA was synthesized using DNA polymerase, and the double-stranded cDNA was purified with a kit. After purifying the double-stranded cDNA, the ends were repaired, the A-tails were attached, ligated with a sequencing adapter, and then the PCR was performed. The sequencing library was used for sequencing. After constructing the library, the range of the inserted fragments in the library was detected using the Agilent 2100 Bioanalyzer, and the library concentration was analyzed using the ABI StepOnePlus Real-Time PCR system. In this study, the Illumina HiSeq sequencer was used to sequence. Software on the sequencing platform is visualized, and the original data in FASTQ format (Raw Data) is obtained. To analyze the sequencing data for further analysis, we use the Cutadapt (v1.15) software to filter out connectors and low-quality reads. The differential expression genes (DEGs) between the control group and $Al(OH)_3$ treatment groups were further analyzed with DEG-seq2 methods. P-value$<$ 0.05 and fold change$>$ 1.5 identified DEGs. A ClusterProfiler package in R studio was used to conduct enrichment analysis for Gene Ontology (GO) and Kyoto Encyclopedia of Genes and Genomes (KEGG). According to the interaction network of the top 10 HUB genes counted by the EPC method, the interactive relationship files were imported into Cytoscape 3.5.0 software and drawn into a network diagram of gene path interaction.

2.10. Quantification of layer thickness and immunofluorescence staining

The thickness of the ventricular zone (VZ) and cortical plate (CP) of the forebrain organoids were measured following the literature (Mariani et al., 2015). Briefly, the VZ was determined by SOX2 staining and the shape of the neural tube; the subventricular zone (SVZ) was outlined from the outer edge of the VZ to the beginning of the CP by SOX2 and TBR2 co-staining. The CP region was outlined outside the VZ to the nearest pial surface and determined by CTIP2 and NeuN staining. The average length of VZ and CP layers was measured at a 45°angle using the Zeiss Axiovision 4.0 system.

The percentage of $SOX2^+$, EdU^+, $TUNEL^+$, and $Ki67^+$ cells to $DAPI^+$ cells in the VZ of day 28 organoids, $TBR2^+$ to $DAPI^+$ cells, and $ki67^+$ to $DAPI^+$ cells in the VZ of day 56 organoids, $SOX2^+$ and $HOPX^+$ cells to $DAPI^+$ cells in the outer SVZ (oSVZ) of day 96 organoids were analyzed by ImageJ. Quantifications of the average MAP2 and S100β fluorescent densities were performed using three sections per organoid, and images were acquired to cover the entire extent of the organoid. MAP2 and S100β fluorescent densities were estimated using Fiji software.

2.11. Inductively coupled plasma-mass spectrometry analyses (ICP-MS)

Al concentrations of the day28 old cerebral organoids were determined by Inductively coupled plasma-mass spectrometry (ICP-MS). We added 8 ml mixed acid (concentrated nitric acid: hydrofluoric acid: perchloric acid=3:3:1) into 0.1–0.15 g cerebral organoids samples and then heated at 250 ℃ until the perchloric acid was exhausted (at this time, the sample has been completely evaporated). When the temperature drops to about 180 ℃, added 8 ml aqua regia and 10 ml of the internal standard mixture while it is hot, mixed them well, and placed them overnight. The next day, 5 ml of 3% nitric acid solution was added into 250ul of digestion solution and mixed well for Inductively coupled plasma-mass spectrometry (ICP-MS, Thermo-X7, Thermo.Co). The performance of the analysis relative to a certified standard was confirmed before testing samples. The result was shown in the supplement material.

2.12. Access of data

All raw sequences were deposited in the NCBI Sequence Read Archive (SRA) under the accession number PRJNA904903.

2.13. Statistical analysis

SPSS 20.0 software was performed for the statistical analysis of all data. The differences in the three groups were analyzed using one-way ANOVA followed Tukey's post-hoc test. The differences between the two groups were analyzed by unpaired t-test. The data were presented as mean±SEM. The significance level was set at $P < 0.05$, and the column figures were processed by GraphPad Prism 9.0.0.

3. Results

Our findings show the first evidence that $Al(OH)_3$ exposure at a specific concentration could induce neurotoxicity and also provide a novel perspective into prevention and alleviation strategies for related diseases caused by $Al(OH)_3$ exposure and also provides a reference for the clinical doses in children safety.

3.1. $Al(OH)_3$ exposure induced cytotoxicity in human ESCs

The impacts of $Al(OH)_3$ treatment on human ESCs cell viability were assessed by CCK8 assays. As Fig. 1C and S5 shows, the cell viability was observed to be significantly affected by 5–100 μg/ml of $Al(OH)_3$ after 24-h treatment compared with the control group (cell viability, 5 μg/ml:90.33% ± 0.03802, 25 μg/ml:84.59% ± 0.01808, 50 μg/ml: 82.23%

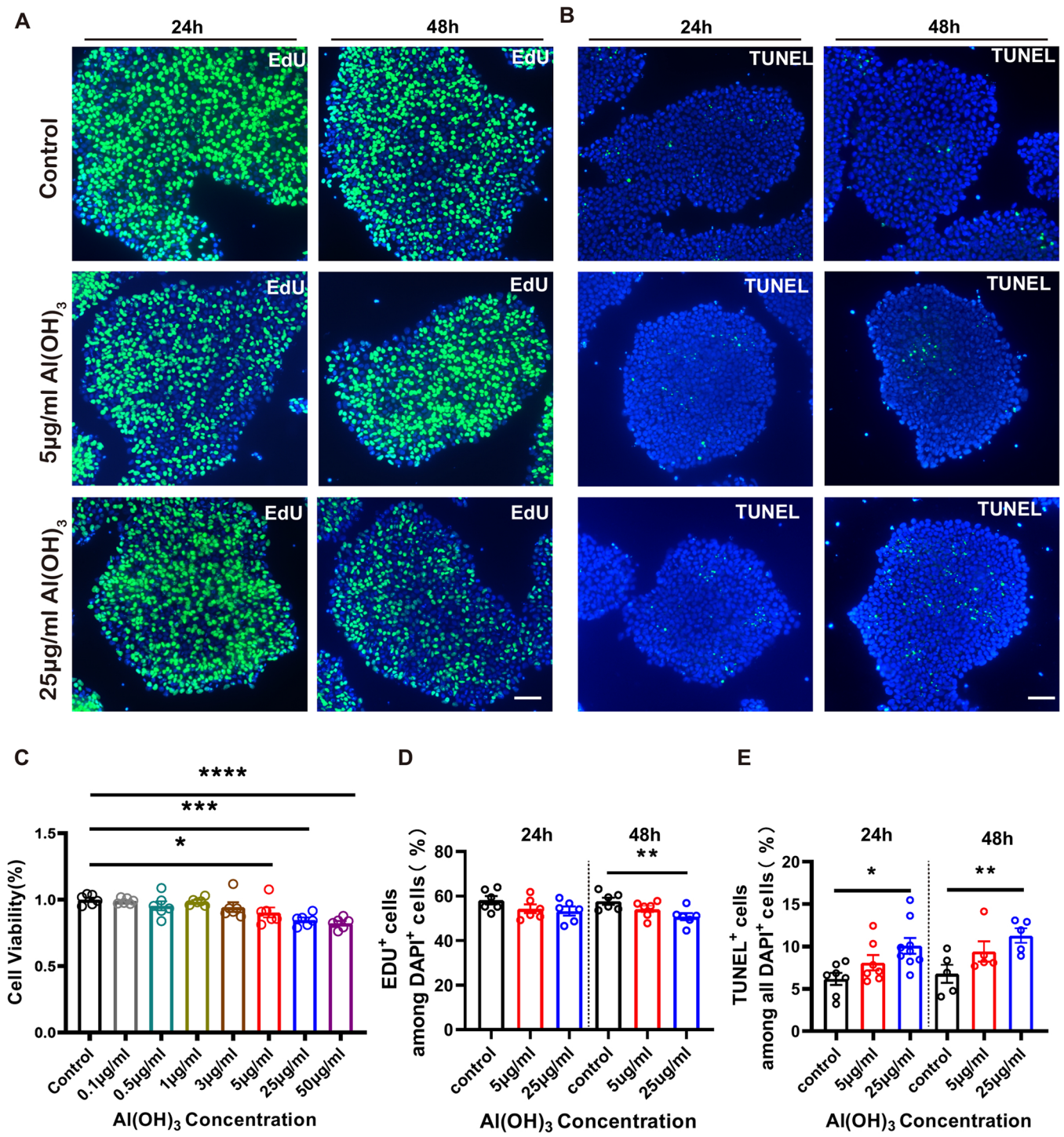

Fig. 1. $Al(OH)_3$ treatment reduced proliferation and cell viability and promoted apoptosis of the human embryonic stem cells. A: Immunostaining images of EdU in hESC of control and $Al(OH)_3$-treatment with 5 and 25 μg/ml concentrations for 24 h and 48 h. Scale bars, 50 μm. B: Immunostaining images of TUNEL in hESC of control and $Al(OH)_3$-treatment with 5 and 25 μg/ml concentrations for 24 h and 48 h. Scale bars, 50 μm. C: CCK-8 assay was performed to determine cell proliferation of hESC after 24 h treated with different concentrations of $Al(OH)_3$. (Values present as the mean±SEM. n = 6, ordinary one-way ANOVA, followed by Tukey post-hoc test. * $P < 0.05$; *** $P < 0.001$; **** $P < 0.0001$). D, E: The ratio of EdU^+ and $TUNEL^+$ cells among $DAPI^+$ cells in hESC clone. (Values present as the mean ±SEM. n ≧ 6, ordinary one-way ANOVA, followed by Tukey post-hoc test. * $P < 0.05$; ** $P < 0.01$).

± 0.01679; 5 μg/ml VS. control, $P < 0.05$; 25 μg/ml VS. control, $P < 0.001$; 50 μg/ml VS. control, $P < 0.0001$, respectively), and no significant effect on cell viability was found at low concentrations below 5 μg/ml (Fig. S5A), and $Al(OH)_3$ above 5 μg/ml could induce cytotoxicity (Fig. S5B). Next, we performed EdU staining to assess cell proliferation. The rate of EdU^+ cells showed a decreasing trend with increasing Al $(OH)_3$ concentration in the 24 h and 48 h exposure groups (Fig. 1A), with a significant difference after 48 h exposure at a concentration of 25 μg/ml (percentage of EdU^+ cells among DAPI cells, 50.71% ± 0.01626, $P < 0.05$) compared to the control group (Fig. 1D, 57.65% ± 0.01587). Meanwhile, TUNEL staining was used to assess cell apoptosis in hESC following $Al(OH)_3$ treatment. The cells were exposed at 0, 5, and 25 μg/

ml $Al(OH)_3$ for 24 h and 48 h. The number of $TUNEL^+$ cells showed an increasing trend with increasing $Al(OH)_3$ concentration in both the 24 h and 48 h exposure groups (Fig. 1B), with a significant increase in $TUNEL^+$ cells after 24 h exposure at a concentration of 25 μg/ml(percentage of $TUNEL^+$ cells among DAPI cells 10.51% ± 0.00926, $P < 0.05$) compared to the control group (Fig. 1E, 6.16% ± 0.00711), and a significant difference in the 48 h exposure group at a concentration of 25 ug/ml (percentage of $TUNEL^+$ cells among DAPI cells, 11.29% ± 0.00853, $P < 0.05$) compared to the control group (Fig. 1E, 6.78% ± 0.01066). Based on the above results of $Al(OH)_3$ exposure, we subsequently focused on the effects of two concentrations of 5, 25 μg/ml $Al(OH)_3$ on cerebral organoids.

3.2. $Al(OH)_3$ treatment reduced NPC proliferation and promoted cell apoptosis in day 28 cerebral organoids

To better recapitulate the features of the developing human cerebral cortex in vitro and investigate the neurotoxicity of $Al(OH)_3$ exposure, human dorsal forebrain organoids were derived from hESCs following Lancaster's differentiation protocol (Giandomenico et al., 2021). According to the developmental pattern, we started $Al(OH)_3$ exposure from day 22 of cerebral organoid development and found that 25 μg/ml concentration caused a significant area difference in cerebral organoids at day 28, while 5 μg/ml concentration did not cause a significant difference (Fig. 2C, D). Based on this result we chose $Al(OH)_3$ exposure for 6 days. The experimental procedure was shown in Fig. 2A. EBs were developed into a neuroectoderm on day 6 and a neuroepithelial lineage on day 14. Expanded neuroepithelial structure and forebrain organoid were formed and observed in phase-contrast images (Fig. 2B). NPCs markers PAX6 and SOX2 are predominantly expressing in the rosette (Fig. S2A, B), and DCX and Tuj1-labeled neurons well localized near the ventricle-like structures (Fig. S2C, D) by immunofluorescence staining of day28 cerebral organoid sections. The cerebral organoids showed intermediate progenitor (IP) cell marker TBR2 in the SVZ on day 28 (Fig. S2E) and 56 (Fig. S2G), scattered $NeuN^+$ labeled neurons in the CP on day 28 (Fig. S2F), stratified deep-layer marker CTIP2 on day 56 (Fig. S2G). We found upper-layer marker SATB2 with CTIP2 emerged in the CP layer on day 96 (Fig. S2H). The gross morphological features of the organoids were photographed to evaluate the effects of $Al(OH)_3$ exposure on the growth of organoids (Fig. 2C). No significant differences in the surface area (Fig. 2D) were found in the organoid with $Al(OH)_3$ exposure at 5 μg/ml(surface area, 2.8105 ± 0.14373 mm^2) compared with control organoids(surface area, 3.2138 ± 0.15719 mm^2) on day 28. However, the organoids after 25 μg/ml treatment showed an apparent smaller surface area (Fig. 2D, 2.6707 ± 0.15207 mm^2, $P < 0.05$) than control organoids until day 28, suggesting a reduction in the organoid size reduced by $Al(OH)_3$ treatment is dose-dependent. To clarify whether Al enters the tissues, we examined the Al content inside the organoid after 6 days of $Al(OH)_3$ exposure using the ICP-MS method, and we could find that the tissue Al content increased with increasing Al $(OH)_3$ concentration (Fig. S6). Histological analysis revealed the cultured cerebral organoids showing unique characteristics of the developing cerebral cortex involving ventricle-like structure. The relative thickness of the VZ layer was quantified by SOX2, which is a marker for NPC (Fig. 2E). We observed well-defined VZ-like structures with padding $SOX2^+$ NPCs near the lumen at day 28 organoids (Fig. 2E). Consistent with reduced organoid size, 25 μg/ml $Al(OH)_3$ exposure treatment caused a massive reduction in the VZ thickness(96.6511 ± 7.66048 μm, $P < 0.05$) and the proportion of $SOX2^+$ cells in the VZ-like areas of day 28 organoids ($P < 0.001$). However, 5 μg/ml Al $(OH)_3$ exposure treatment caused a substantial reduction in the proportion of $SOX2^+$ cells in the VZ-like areas($P < 0.05$) and had decreased trend but no significance in the VZ thickness(114.9920 ± 8.71129 μm, $P > 0.05$) compared to the control organoid (Fig. 2E, G).

To determine the causes of the reduced NPC pool in $Al(OH)_3$ treated organoids, EdU and Ki67 were performed to detect the proliferation of NPCs. Ki67 immunostaining revealed that 25 μg/ml $Al(OH)_3$ treated organoids displayed a decrease in the percentage of $Ki67^+$ cells in the VZ ($P < 0.01$), whereas 5 μg/ml $Al(OH)_3$ exposure did not markedly alter the ratio of $Ki67^+$ cells in the VZ (Fig. 2F, H). Similarly, The ratio of EDU^+ cells was decreased markedly with exposure of 25 μg/ml Al $(OH)_3$($P < 0.05$) but did not change in 5 μg/ml $Al(OH)_3$ group compared to the control group (Fig. 2F, I). TUNEL assay was performed to examine the apoptosis status of the cells. We further found a significant increase of $TUNEL^+$ cells in the VZ-like regions of 5 μg/ml and 25 μg/ml $Al(OH)_3$ treated organoids (Fig. 2F, J). Therefore, these results suggested that 5 μg/ml($P < 0.01$) and 25 μg/ml($P < 0.001$) $Al(OH)_3$ treatment decreased the NPC pool as it inhibited the proliferation and promoted apoptosis. Notably, 5 μg/ml $Al(OH)_3$ treatment typically promoted its apoptosis and did not alter NPC proliferation.

3.3. $Al(OH)_3$ exposure changes gene expression in cerebral organoids

The bulk RNA-seq was conducted to investigate the DEGs on day 28 cerebral organoids to uncover the underlying mechanisms of $Al(OH)_3$-treatment-induced neurotoxicity. Using hierarchical clustering, the gene expression profiles between the control and 5 μg/ml $Al(OH)_3$ were shown on the heatmap (Fig. 3A) and the control and 25 μg/ml $Al(OH)_3$ (Fig. 3B). We identified 535 and 934 DEGs in the organoids treated with 5 and 25 μg/ml $Al(OH)_3$, respectively. Volcano plots showed 245 upregulated and 290 downregulated DEGs in the 5 μg/ml group (Fig. 3B), but 226 upregulated and 708 downregulated DEGs in the 25 μg/ml group (Fig. 3D). These two sets of DEGs were further used in the subsequent analyses. GO enrichment was conducted on 535 DEGs in the 5 μg/ml group, which showed that these genes could be significantly enriched in multiple biological processes, such as embryonic organ development, forebrain development, neural tube patterning, cell fate commitment, and cell fate specification (Fig. 3E). To explore the core genes underlying the effects, we constructed an interaction network map between genes and go terms (Fig. 3F). As the map of the gene-concept network showed, *PTCH1* was in the center of the network, which was critical in cell proliferation(Shikata et al., 2011). Increased *PTCH1* in the cerebral organoid exposed to 5 μg/ml $Al(OH)_3$ might explain reduced $SOX2^+$ NPC in the VZ.

Additionally, for the functional analysis of the 934 DEGs in the 25 μg/ml $Al(OH)_3$-treated group, the enriched GO terms mainly included regulation of nervous system development, regulation of cell growth, regulation of cell development, forebrain development, regulation of neurogenesis, and central nervous system neuron differentiation (Fig. 3G). At the same time, we also analyzed the interaction network in GO biological process category and further identified *WNT3A* as the bridge gene connected in these pathways and involved in NPC depletion in the 25 μg/ml $Al(OH)_3$-treated cerebral organoid (Fig. 3H).

3.4. Enrichment of Hippo signaling pathway involved in the reduction of NPC pool in the $Al(OH)_3$ treated day28 organoids

Significant enrichment in the KEGG pathway was further performed on 535 DEGs in the 5 μg/ml group and showed to be associated with ECM-receptor interaction, neuroactive ligand-receptor interaction, hippo signaling pathway, focal adhesion, and signaling pathways regulating pluripotency of stem cells (Fig. 4A). For the 934 DEGs in the 25 μg/ml $Al(OH)_3$ group, the top 20 KEGG pathways consist of the Wnt signaling pathway, neuroactive ligand-receptor interaction, and hippo pathway (Fig. 4B). Hippo signaling regulates cell proliferation, apoptosis, and stem cell self-renewal to control organ size in evolutionarily conserved ways (Reuven et al., 2013). The hierarchical clustering heatmap showed Hippo signaling pathway appeared in both groups (Fig. 4C). We selected the top 10 Hub genes in the Hippo signaling way by EPC method (Fig. 4D). Among these top 10 interacting genes, there were nine down-regulated hub genes, *WNT1*, *WNT3A*,

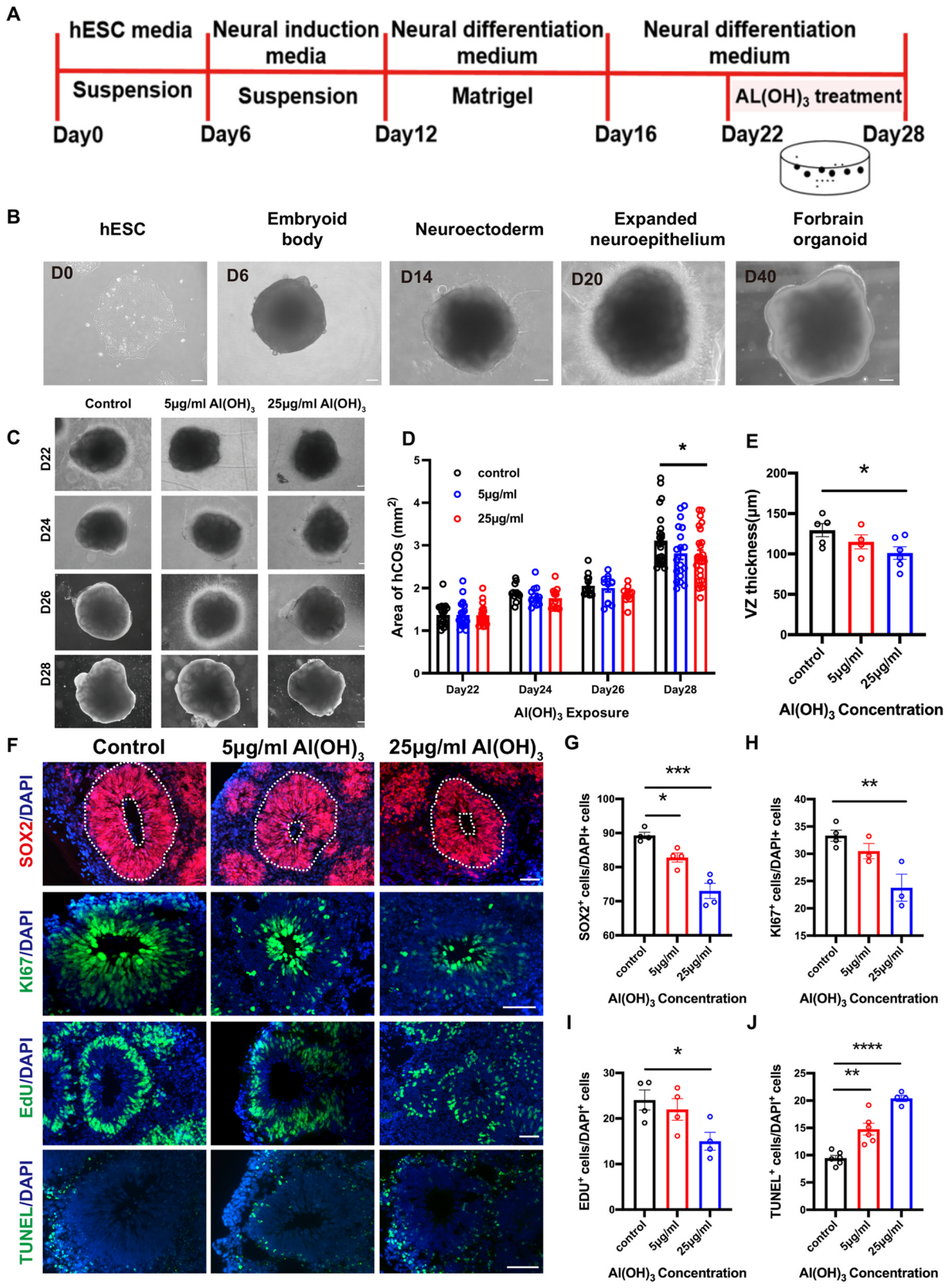

Fig. 2. $Al(OH)_3$ exposure impaired the development of day28-old cerebral organoids. A: A schematic diagram of the experimental configuration. B: Representative images showing the organoid growth from day0 to day40. Scale bars, 100 μm.C: Representative bright-field view of three parallel groups before and after treatment with $Al(OH)_3$ treatment at concentrations of control(0), 5, and 25 μg/ml for six days, respectively. Scale bars, 100 μm. D: Quantification of day22–28-old cerebral organoids size based on area. E: Qualification of VZ thickness based on SOX2 staining. F: Immunostaining for SOX2(red), Ki67(green), EdU(green), and TUNEL (green) in day28-old cerebral organoids. Scale bars, 50 μm. G-J: The statistical analysis of $SOX2^+$ cell, $Ki67^+$ cell, EdU^+ cell, and $TUNEL^+$ cell ratio of the DAPI cells in the VZ of organoids in three groups after six days of treatment with different $Al(OH)_3$ concentrations. Data are shown as mean±SEM; ($n \geq 9$ VZ-like structures from at least three organoids, ordinary one-way ANOVA, followed by Tukey post-hoc test. * $P < 0.05$; ** $P < 0.01$; *** $P < 0.001$).

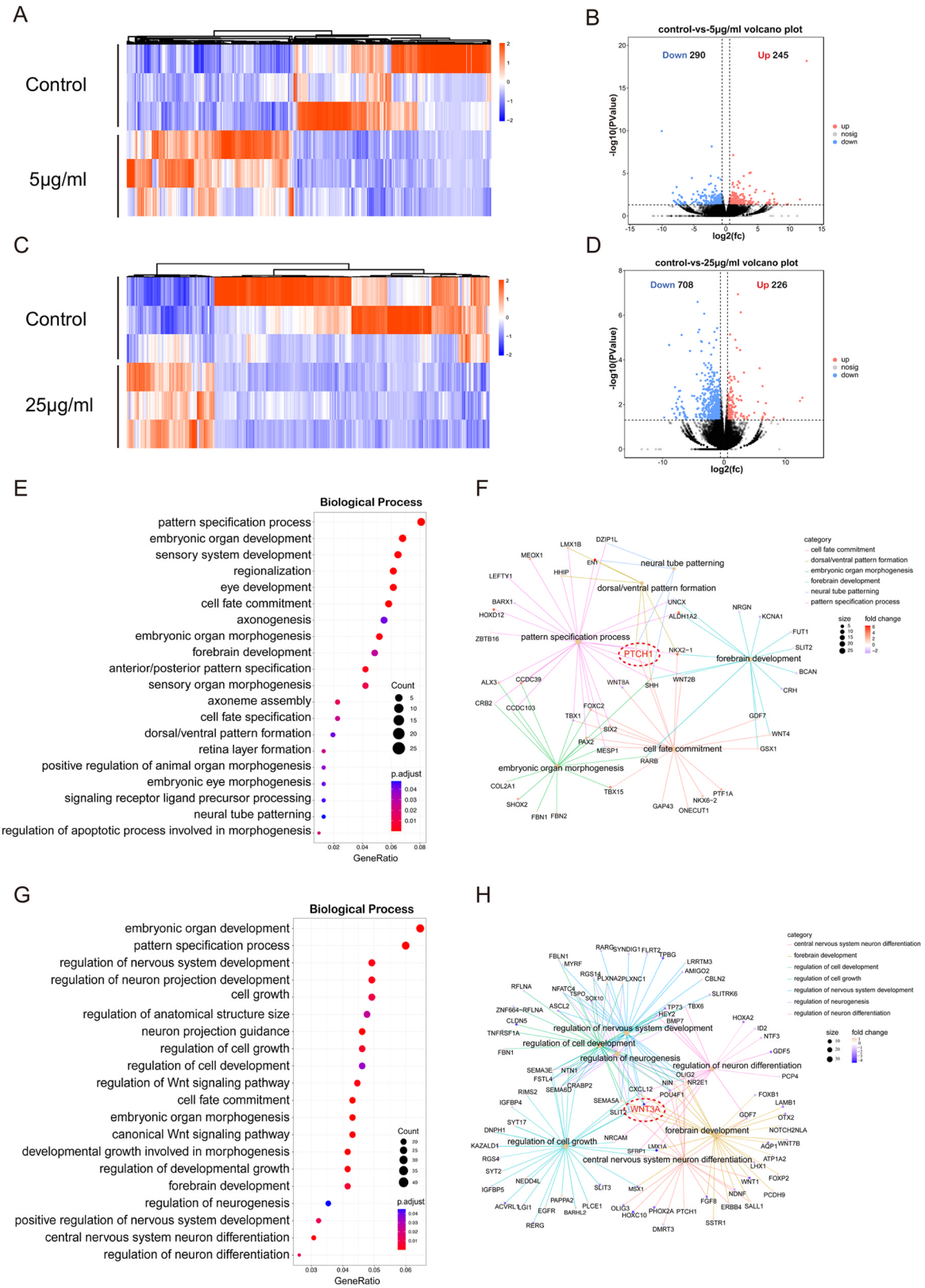

Fig. 3. Transcriptomes comparison showed that 5 and 25 μg/ml $Al(OH)_3$ treatment exerted different effects on cerebral organoids. A: Heatmap of DEG expression in the three groups. B: Volcano plot of the control group compared with 5 μg/ml $Al(OH)_3$ treated group. C: Volcano plot of the control group compared with 25 μg/ml $Al(OH)_3$ treated group. D: GO enrichment bubble plots of DEGs between the control group and 5 μg/ml $Al(OH)_3$ treated group. E: The Gene-Concept Network of GO enrichment of DEGs between the control group and 5 μg/ml $Al(OH)_3$ treated group. F: GO enrichment bubble plots of DEGs between the control group and 25 μg/ml $Al(OH)_3$ treated group. G: The Gene-Concept Network of GO enrichment of DEGs between the control group and 25 μg/ml $Al(OH)_3$ treated group.

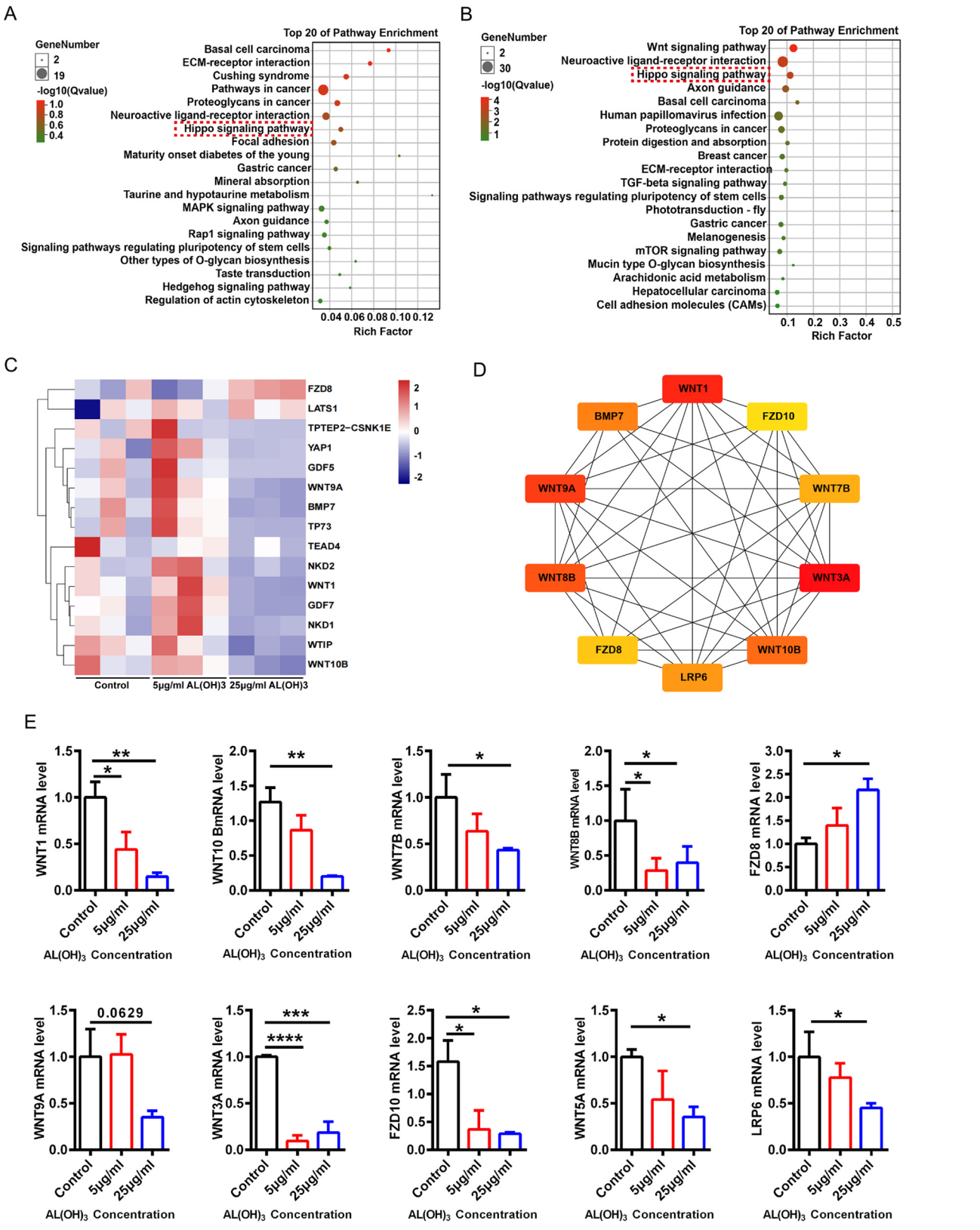

Fig. 4. The KEGG enrichment analysis of $Al(OH)_3$ induced DEGs-related pathways. A, B: The KEGG enrichment analyses were used to identify the top 20 pathways of DEGs in control vs 5 μg/ml(A) and control vs 25 μg/ml(B), separately. Red represents a high degree of enrichment, green is the opposite, and the bubble size represents the number of DEGs. Among all pathways in KEGG analysis, the hippo signaling pathway is more significant and appeared in both groups. C: The heat map shows $Al(OH)_3$ changed DEGs related to the hippo signaling pathway. D: Top ten HUB gene network map obtained by EPC method. E: The mRNA levels of *WNT1, WNT10B, WNT7B, WNT8B, FZD8, WNT9A, WNT3A, FZD10, WNT5A*, and *LRP6* of cerebral organoids with $Al(OH)_3$ treatment were detected by RT-PCR. Data are shown as mean±SEM (n ≧ 3 for each group, ordinary one-way ANOVA, followed by Tukey posthoc test. ** $P < 0.01$, *** $P < 0.001$, **** $P < 0.0001$).

WNT9A, *WNT7B*, *WNT8B*, *WNT10B*, Bone Morphogenetic Protein 7 (*BMP7*), Frizzled Class Receptor 10 (*FZD10*), and LDL Receptor Related Protein 6 (*LRP6*). The up-regulated hub gene *FZD10* connected to different communities (Fig. 4E). These results suggested that 5 μg/ml and 25 μg/ml $Al(OH)_3$ induced neurotoxicity by impairing the Hippo signaling pathway.

Annotation of the KEGG pathway in $Al(OH)_3$-exposed cerebral organoids showed DEGs could be categorized into five terms: organismal systems, metabolism, human diseases, environmental information processing, and cellular processes (Fig. 5A, B; S4A, B). The environmental information processing term enriched with the highest proportion of genes (Fig. S3A, B). We made a protein interaction network using STRING for 92 genes related to seven environment-related pathways. The protein interaction between the Wnt signaling pathway and the Hippo signaling pathway is more evident in 25 μg/ml $Al(OH)_3$ exposure (Fig. 5C). In the case of 5 μg/ml $Al(OH)_3$ exposure, a protein interaction network using STRING for all 43 genes of six environment-related pathways showed the Hippo signaling pathway is essential in the network diagram (Fig. S4C). The Hippo signaling pathway was identified as a significant pathway involved in the environmental information process for the 5 μg/ml and 25 μg/ml $Al(OH)_3$ treatments relative to controls.

YAP, a major downstream effector of the Hippo pathway, is closely associated with the proliferation of progenitor cells. We found that 5 μg/ml and 25 μg/ml $Al(OH)_3$ sharply decreased the YAP1 expression in the $SOX2^+$ aRGs (Fig. 6A). As expected, 25 μg/ml $Al(OH)_3$ treated cerebral organoids displayed a marked reduction in the YAP1 mRNA level compared with control organoids ($P < 0.05$), but 5 μg/ml $Al(OH)_3$ treatment caused a decreased trend of YAP1 mRNA level in the cerebral organoid (Fig. 6C, $P = 0.055$). Similarly, western blotting showed that the expression of YAP1 protein was significantly different among the three groups, in which the 5 μg/ml and 25 μg/ml $Al(OH)_3$ treated cerebral organoids showed a markedly decreased YAP1 level compared with the control group (Fig. 6B, D, $P < 0.01$). LATS1/2, an upstream effector of YAP1, potentially restricts YAP1 to the cytoplasm and priming for degradation. We further identified that the expression of LATS1/2 protein was significantly different among the three groups, in which 5 μg/ml and 25 μg/ml $Al(OH)_3$ treated cerebral organoids showed a markedly increased creased LATS1/2 level compared with the control group (Fig. 6B, E, $P < 0.001$). These results suggested that down-regulation of Hippo-YAP1 might contribute to decreased NPCs and higher apoptosis in $Al(OH)_3$ treated cerebral organoids compared with the control.

3.5. Early 25 μg/ml $Al(OH)_3$ exposure inhibited NPC proliferation but promoted neuron differentiation in day 56 cerebral organoids

As the biological analysis shows, $Al(OH)_3$ exposure had the potential to affect neuron differentiation in cerebral organoids. To further understand the effect of $Al(OH)_3$ exposure on neuron differentiation, the distributions of NPCs and neurons were analyzed in 56-day organoids (Fig. 7A). No significant differences in the surface area (Fig. 7B, 4.703 ± 0.38917 mm^2, $P > 0.05$) and radius (Fig. 7C, 1.1624 ± 0.0755 mm , $P > 0.05$) were found in the organoid with $Al(OH)_3$ exposure at 5 μg/ml compared with control organoids (5.0862 ± 0.2322 mm^2, 1.2959 ± 0.03113 mm). However, the organoids with 25 μg/ml $Al(OH)_3$ treatment displayed markedly smaller surface area (4.0932 ± 0.24608 mm^2, $P < 0.05$) and radius (1.2154 ± 0.02678 mm, $P < 0.05$) than the control organoids at day 56, indicating a dose-dependent reduction in organoid size induced by $Al(OH)_3$ treatment. Consistent with reduced organoid size, 25 μg/ml $Al(OH)_3$ treatment caused a significant reduction in the VZ thickness of day56 organoids (95.0067 ± 9.9993 μm, $P < 0.05$), but 5 μg/ml $Al(OH)_3$ treated organoids were not significantly changed in the VZ thickness (109.1842 ± 17.1037 μm, $P > 0.05$) (Fig. 7D, E). At this stage, TBR2 staining recognizing SVZ showed that SVZ thickness and the proportion of $TBR2^+$ cells in the SVZ-like areas were comparable between the control group and $Al(OH)_3$-exposed groups (Fig. 7D, F, G). Ki67 immunostaining revealed that 25 μg/ml $Al(OH)_3$ treatment caused a substantial reduction in the percentage of Ki67 positive cells in the VZ (Fig. 7D,H, $P < 0.01$), whereas 5 μg/ml $Al(OH)_3$ did not markedly alter the ratio of Ki67 positive cells in the VZ (Fig. 7D, H, $P > 0.05$).

Furthermore, the deep-layer neuron marker CTIP2 and the mature neuron marker NeuN in the CP-like regions of day 56 organoids were examined. We measured the thickness of the CP-like area with CTIP2 stained neurons and found that 25 μg/ml $Al(OH)_3$ exposure significantly increased the CP-like area thickness (142.1664 ± 12.36026 μm, $P < 0.05$) compared to the control group (93.5296 ± 7.14292 μm) (Fig. 7I, K). The CP-like area could also be distinguished by $NeuN^+$ cells, and the NeuN staining showed that there was a thicker CP-like area in 25 μg/ml $Al(OH)_3$ group (104.6815 ± 8.5331 μm, $P < 0.05$) compared with the control group (75.0238 ± 4.06337 μm) (Fig. 7J, L). As expected, the mRNA levels of *SOX2* and *NESTIN* (neuroepithelial stem cell marker) were markedly inhibited by 25 μg/ml $Al(OH)_3$ exposure ($P < 0.05$, $P < 0.01$), and the mRNA level of CTIP2 was significantly increased in 25 μg/ml $Al(OH)_3$ group compared to the control group (Fig. 7M, $P < 0.05$). TBR2 mRNA level showed an increasing trend in the $Al(OH)_3$ groups. These results suggested that $Al(OH)_3$ exposure could decrease NPC proliferation but promote premature neural differentiation.

3.6. $Al(OH)_3$ exposure at 25 μg/ml on day 96 decreased oRG cells and promoted astrocyte differentiation

To further investigate the consequence of chronic 25 μg/ml $Al(OH)_3$ exposure at day 90, the distributions of oRGs in 96-day organoids were analyzed. The day96 cerebral organoids contained a distinct $SOX2^+$/$HOPX^+$ oSVZ-like layer exhibiting unipolar morphology of oRGs with radially oriented basal processes toward the pial surface (Fig. 8A). We found the ratios of $SOX2^+$ and $HOPX^+$ to $DAPI^+$ cells were decreased by 25 μg/ml $Al(OH)_3$ treatment, suggesting it inhibited the formation of oRGs in the oSVZ- like structures (Fig. 8C, D, $P < 0.01$, $P < 0.001$).

Next, we performed the immunostaining of neuron marker MAP2 and astrocyte marker S100β in day 96 cerebral organoid (Fig. 8B). We found that the mean fluorescent intensity of MAP2 was similar between the control and 25 μg/ml $Al(OH)_3$-treated group (Fig. 8F), the mean fluorescent intensity of S100β was significantly increased in 25 μg/ml Al(OH)3 treated group compared to the control group (Fig. 8E, $P < 0.05$). These results illustrated that 25 μg/ml $Al(OH)_3$ exposure in the late stage could inhibit the proliferation of oRGs, but trigger a higher rate of astrocyte differentiation (Li et al., 2021).

4. Discussion

In the present study, we utilized dorsal forebrain organoids generated from hESCs to analyze the impact of $Al(OH)_3$ exposure at early and later stages on cortical development. We found that $Al(OH)_3$ exposure at an early stage inhibited proliferation and promoted apoptosis of $SOX2^+$ NPCs, contributing to a corresponding reduction in gross organoid volume in higher concentrations of $Al(OH)_3$ treated organoids. Importantly, we identified the impaired Hippo-YAP1 signaling as a possible mechanism for the depletion of the NPC pool induced by $Al(OH)_3$ exposure to early-stage forebrain organoids. We noticed that $Al(OH)_3$ exposure at an early stage dampened NPC proliferation and promoted neuron differentiation in day 56 organoids. Of note, we further showed that higher concentrations of $Al(OH)_3$ exposure at a later stage caused reduced oRG output and increased astrocytes. Our studies highlight new insights into the pathogenesis of neurotoxicity induced by Al(OH)3 exposure. As far as we know, this is the first study to report the neurotoxicity and molecular mechanism of $Al(OH)_3$ exposure during human early cerebral cortex development.

Several studies reported that $Al(OH)_3$ exposure could be neurotoxic

A

ID	Description
ko00512	Mucin type O-glycan biosynthesis
ko00590	Arachidonic acid metabolism
ko04310	Wnt signaling pathway
ko04080	Neuroactive ligand-receptor interaction
ko04390	Hippo signaling pathway
ko04512	ECM-receptor interaction
ko04350	TGF-beta signaling pathway
ko04150	mTOR signaling pathway
ko04514	Cell adhesion molecules
ko04550	Signaling pathways regulating pluripotency of stem cells
ko04360	Axon guidance
ko04974	Protein digestion and absorption
ko04745	Phototransduction
ko04916	Melanogenesis
ko05217	Basal cell carcinoma
ko05165	Human papillomavirus infection
ko05205	Proteoglycans in cancer
ko05224	Breast cancer
ko05226	Gastric cancer
ko05225	Hepatocellular carcinoma

B

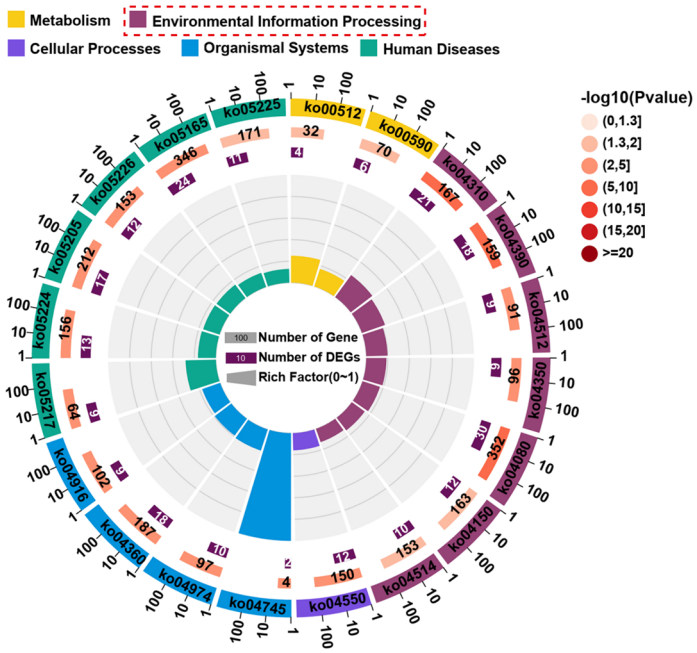

C

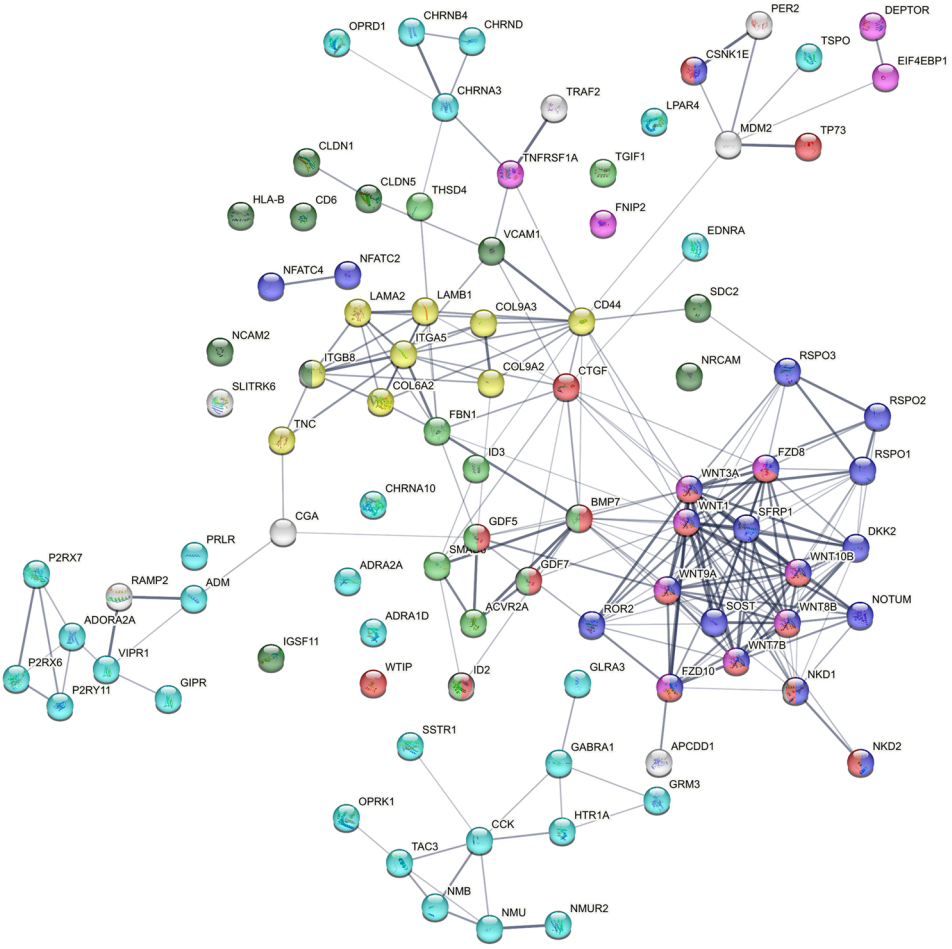

(caption on next page)

Fig. 5. Analysis of key pathways of cerebral organoids exposed to 25 μg/ml $Al(OH)_3$. A: The top 20 KEGG pathways classification table. B: Circle diagram of top 20 enrichment pathways of cerebral organoids exposed to 25 μg/ml $Al(OH)_3$. The first circle shows the number of enriched terms and associated genes, the second circle shows the number of genes in the genomic background and -log10(p-value) for enrichment, the third circle shows the number of DEGs, and the fourth circle shows the enrichment factor. C: All 92 DEGs interaction networks in the Environmental Information Processing classification of the KEGG enrichment top 20 pathways based on the STRING (11.5) database. Dark blue indicates DEGs associated with the Wnt signaling pathway, red indicates DEGs involved in the Hippo signaling pathway, light green indicates DEGs associated with the TGF-β signaling pathway, yellow indicates DEGs involved in ECM-receptor interaction, light blue indicates DEGs involved in Neuroactive ligand-receptor interaction, purple indicates DEGs involved in the mTOR signaling pathway, and dark green indicates DEGs involved in Cell adhesion molecules.

under some conditions, and adjuvant utilization has been implicated in neurological disease (Mold et al., 2020; Niu, 2018; Principi and Esposito, 2018). Different scales of $Al(OH)_3$ may have distinct effects on brain development. Our research focuses on micron-level aluminum hydroxide materials. According to reported studies, exposure to bulk $Al(OH)_3$ and nano $Al(OH)_3$ adjuvants could both cause pathological lesions on the histology sections of the liver, lung, heart, and kidney tissue, but bulk $Al(OH)_3$ adjuvant vaccine had a higher pathological response and a lower total DNA content than $Al(OH)_3$ nanoparticles adjuvant vaccine. Thus, the nano $Al(OH)_3$ may result in less pronounced toxicity, as well as systemic inflammation, compared to the bulk $Al(OH)_3$ in neonatal mice (Hamza Fares et al., 2022). Meanwhile, it is reported in the literature that nano $Al(OH)_3$ particles cause a less inflammatory reaction at the injection site than the traditional $Al(OH)_3$ microparticle forms of 1–20 μm (Li et al., 2014). An animal study has confirmed that Al exposure at 900 and $\geq$ 900 ppm via drinking water from day 6 of pregnancy to day 21 postpartum caused exhaustion of the NSC pool in mice (Inohana et al., 2018). Some studies also observed decreased cell proliferation and increased apoptosis in mouse embryonic NPCs after different concentrations (1, 10, and 50 mM) of Al ions exposure for 48 h. Al ions reduce the numbers and diameters of the neurosphere by inhibiting neurosphere growth (Reichert et al., 2019). In line with this study, in vitro model of dorsal forebrain organoid exposure to a higher concentration of $Al(OH)_3$ from day 22 for six days displayed the reduced size of cerebral organoids. After 6 days of $Al(OH)_3$ exposure, we examined the overall aluminum content of the organoid and could see that it is indeed aluminum that acts after being absorbed into the organoid interior and that there is a significant dose effect. We also noticed a significantly decreased ratio of $SOX2^+$ NPCs in the VZ by 5 μg/ml and 25 μg/ml $Al(OH)_3$ exposure, while only 25 μg/ml $Al(OH)_3$ exposure reduced the ratios of $Ki67^+$ and EdU^+ NPCs in the VZ-like area reflecting inhibition of NPC proliferation. Notably, 5 μg/ml and 25 μg/ml $Al(OH)_3$ exposure caused proapoptotic influence on NPCs. These observations suggest that 25 μg/ml $Al(OH)_3$ treatment decreased the NPC pool by inhibiting the proliferation of NPC and promoting its apoptosis. However, 5 μg/ml $Al(OH)_3$ reduced the NPC pool due to apoptosis in the NPC, suggesting that the effect of $Al(OH)_3$ exposure on brain development appears to be concentration dependent in this organoid model.

Cortical organoids reproduce major structural features of the fetal brain (Lancaster et al., 2013). It is well confirmed that the cerebral cortex in the human brain is characterized by a distinctly stratified cortical structure (Reichert et al., 2019). Using 56-day dorsal cortical organoids, we measured the distribution of progenitor cells and deep-layer neurons. We found that only 25 μg/ml $Al(OH)_3$ exposure dampened the NPC pool and increased the thickness of the CP-like area by staining CTIP2 and NeuN. Typically, both 5 μg/ml and 25 μg/ml Al $(OH)_3$ exposure did not affect the production of IP cells. It seemed that 25 μg/ml $Al(OH)_3$ exposure might promote differentiation at the expense of NPC depletion, leading to a smaller size in the cerebral organoid.

It is well documented that oSVZ-like progenitor layers formed by oRGs are the predominant NPC-producing upper-layer cortical neurons in the developing human cortex (Qian et al., 2019). The appearance of oRG cells at day 70 has been confirmed, and they are increased with cerebral organoid development over time (Bershteyn et al., 2017). To further explore $Al(OH)_3$ exposure at a later stage, day 90 to day 96 was used in this study. The human cerebral cortex encompasses the expanded oSVZs with massive populations of oRGs and is responsible for generating upper-layer neurons during human cortex development (Li et al., 2017). Our analyses showed a well-developed oSVZ with oRGs at day 96 organoids. There was a drastic reduction in the thickness of the oSVZ-like structure accompanied by a reduced ratio of $SOX2^+$ cells and $HOPX^+$ cells in the organoids exposed to 25 μg/ml $Al(OH)_3$. Studies have reported that Al-treated mice increased the proliferation of reactive astrocytes and microglial within the spinal cord and cortex. As expected, we found 25 μg/ml $Al(OH)_3$ exposure could specifically inhibit the output of oRGs and increase the production of astrocytes. Importantly, premature neuronal differentiation was not observed, suggesting 25 μg/ml $Al(OH)_3$ exposure at different stages caused different effects.

RNA-seq data analysis of cerebral organoids also revealed that DEGs were closely associated with neurodevelopmental dysfunction at early stages. GO biological process analysis revealed that $Al(OH)_3$ exposure could affect the pattern specification process, embryonic organ development, and forebrain development. KEGG enrichment analysis further found the Hippo signaling pathway contributes to impaired cerebral cortex development induced by $Al(OH)_3$ exposure. The Hippo signaling pathway, as a highly conserved pathway, is involved in tissue development and regeneration. It can control organ size by regulating cell proliferation and apoptosis (Dong et al., 2007; Huang et al., 2005; Ramos and Camargo, 2012). Evidence has documented that a high level of YAP, the major downstream effector of the Hippo pathway, is involved in the proliferation of basal progenitors derived from apical RGs (aRGs) (Lavado et al., 2021a; Lodge et al., 2019). Recent studies have indicated YAP1 is expressed in RGCs undergoing dynamic changes during cortex development (Jabali et al., 2022; Lavado et al., 2021b; Terry and Kim, 2022). YAP1 was highly expressed in the $SOX2^+$ aRGs located on the apical side of the developing VZ (Zhao et al., 2022). We detected high expression of YAP1 in RGCs of day 28 cerebral organoids, which was decreased by $Al(OH)_3$ exposure. Alterations in the Hippo signaling pathway induced by $Al(OH)_3$ exposure have been confirmed at both mRNA and protein levels. Thus, the impaired Hippo signaling pathway explains the underlying mechanism of the consequence of Al $(OH)_3$ exposure to a cerebral organoid. All these findings help to explain the toxic effects of higher concentration of $Al(OH)_3$ exposure and reveal much detail about previously unreported aspects of abnormal neural development in humans.

5. Conclusions

In summary, the present study revealed the potential toxicity of Al $(OH)_3$ to different stages of human brain development after early exposure via hESC-derived dorsal forebrain organoids. We demonstrated that $Al(OH)_3$ at a dose of 25 μg/ml may produce multifaceted developmental toxicity on the proliferation and differentiation of NPCs, which showed decreased NPC pool at the early and late stages and excessive differentiation at the late stage. Transcriptomic analysis indicated that $Al(OH)_3$ exposure caused early and late-stage NPC reduction and premature neuron differentiation via the inhibited Hippo pathway. We highlight the Hippo-YAP1 involved in $Al(OH)_3$-induced neurotoxicity. Collectively, these new findings elucidate a wide range of changes in biological events that occurred in the $Al(OH)_3$ treated cerebral organoids and provide new insights into the mechanistic link between the elaborate mechanisms.

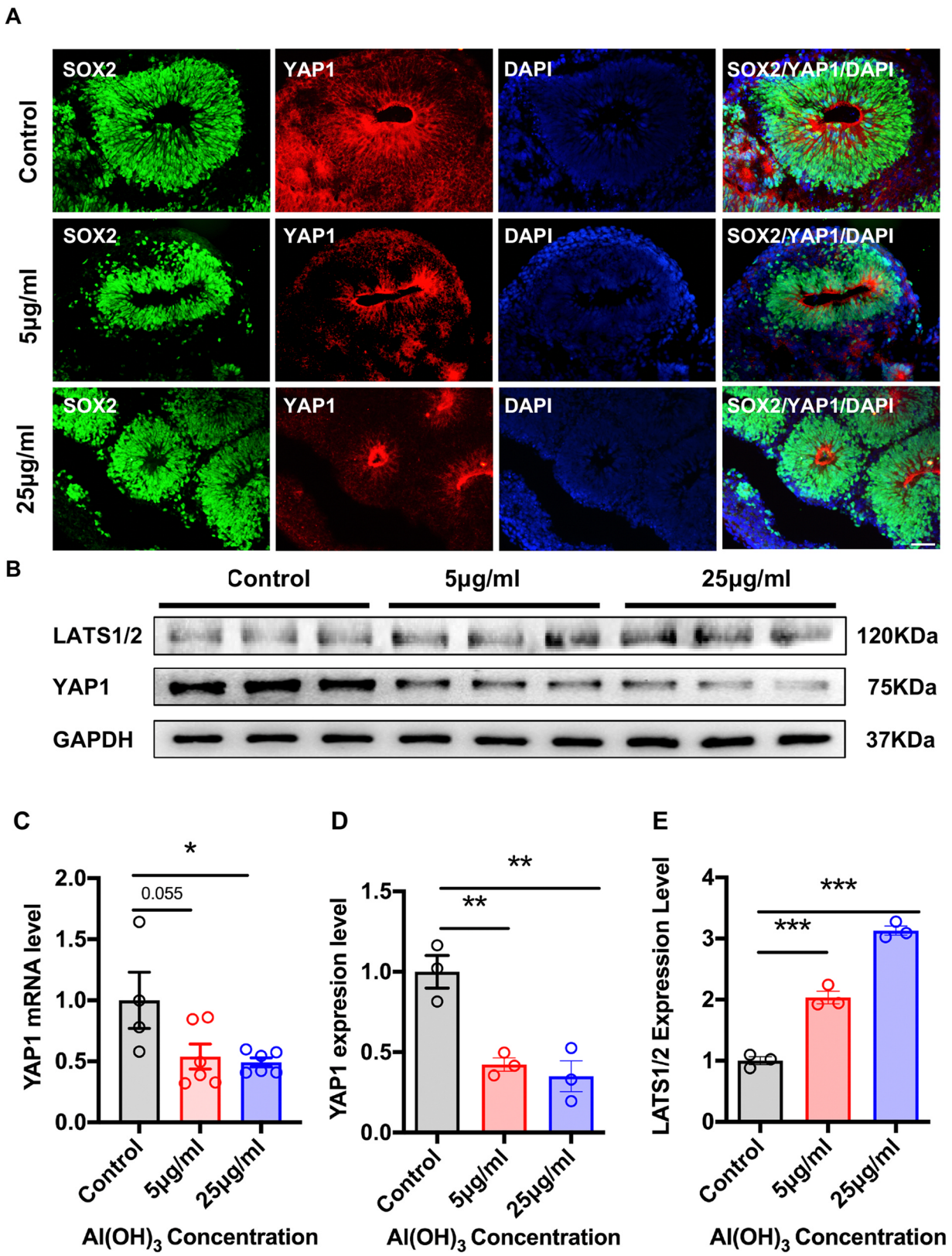

Fig. 6. $Al(OH)_3$ exposure disrupts the Hippo-YAP1 signaling pathway in the day28-old cerebral organoids. A: Immunostaining for SOX2 and YAP in day28-old cerebral organoids after 6 days of treatment with $Al(OH)_3$ (0, 5 μg/ml and 25 μg/ml). Scale bars, 50 μm. B: Representative immunoblots of LATS1/2, YAP1, and GAPDH in cerebral organoids of control, 5 μg/ml and 25 μg/ml $Al(OH)_3$ groups. C: Qualification of relative expression of YAP1 mRNA in cerebral organoids. D, E: Qualification of relative expression of YAP1(D) and LATS1/2(E) in control, 5 μg/ml, and 25 μg/ml $Al(OH)_3$ groups. Data are shown as mean±SEM (n = 3 for each group, ordinary one-way ANOVA, followed by Tukey post-hoc test. * $P < 0.05$, ** $P < 0.01$, *** $P < 0.001$).

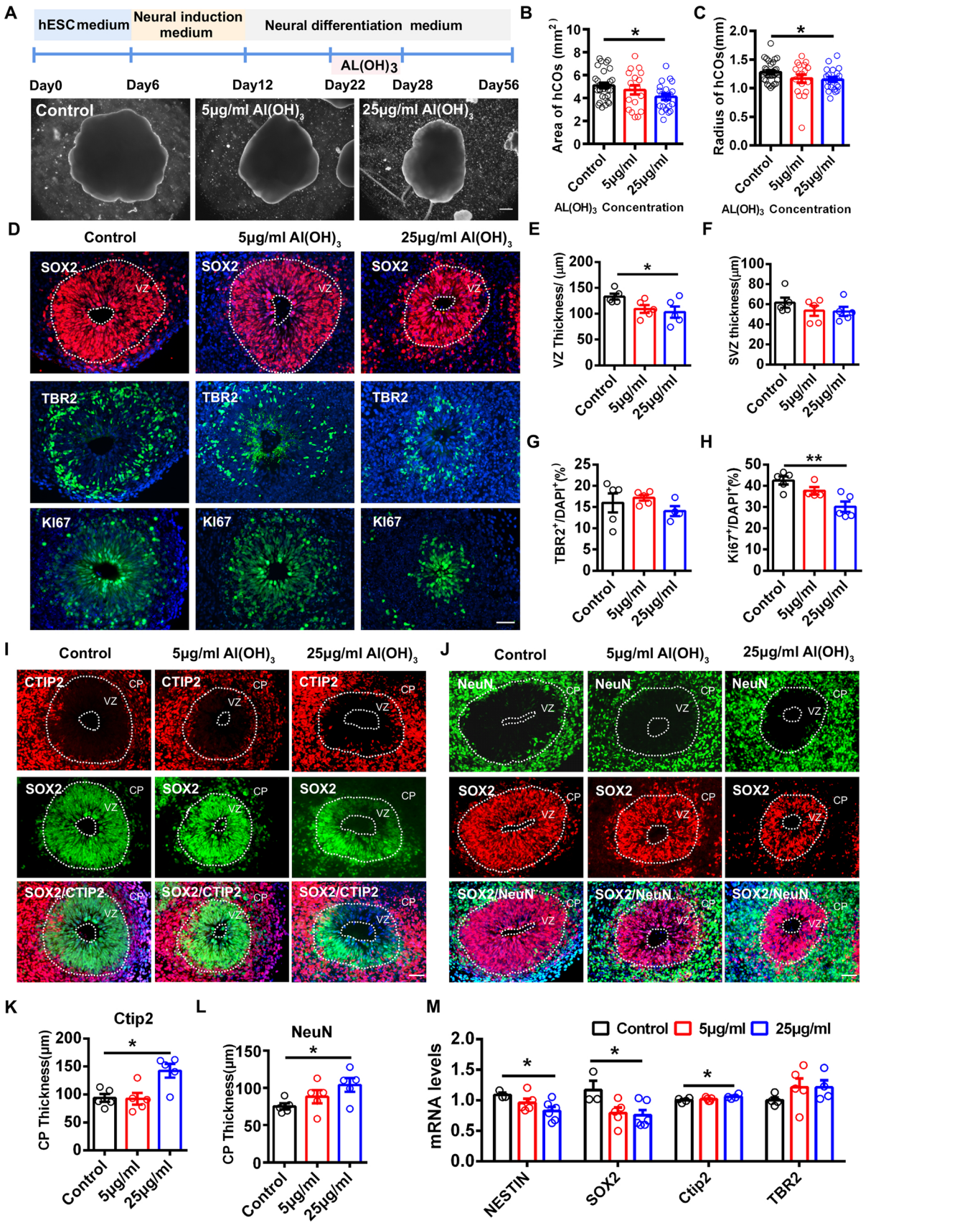

(caption on next page)

Fig. 7. Effects of $Al(OH)_3$ treatment on the NPC proliferation and differentiation of day56-old cerebral organoids. A: Schematic diagram of cerebral organoid culture and representative bright-field image of day56-old cerebral organoids. Scale bars, 100 μm. B, C: The growth of the cerebral organoid was assessed using surface area (B) and radius (C) at day 56. Data are shown as mean±SEM. (n ≧ 15, ordinary one-way ANOVA, followed by Tukey posthoc test. * $P < 0.05$). D: Immunostaining for SOX2(red), TBR2(green), and KI67(green) in the cerebral organoids after six days of treatment with Al(OH)3 (0, 5, and 25 μg/ml). Scale bars, 50 μm. E, F: Quantification of the VZ(E) and SVZ(F) thickness based on SOX2 and TBR2 staining. G, H: Quantification of $TBR2^+$ cells(G) and $KI67^+$ cells(H) to $DAPI^+$ cells at the VZ area in cerebral organoids of control(0), 5 and, 25 μg/ml $Al(OH)_3$ groups. Data are shown as mean±SEM. (n = 5, ordinary one-way ANOVA, followed by Tukey post-hoc test. ** $P < 0.01$). I: Representative images of 0, 5, and 25 μg/ml Al(OH)3 treated human cerebral organoids for SOX2 (green), Ctip2 (red), and DAPI(blue) at day 56. Scale bar, 50 μm. J: Representative images of 0, 5, and 25 μg/ml Al(OH)3 treated human cerebral organoids for SOX2(red), NeuN(green), and DAPI(blue) at day 56. Scale bar, 50 μm. K, L: Quantification of the CP thickness based on CTIP2 (K) and NeuN (L) staining. Data are shown as mean±SEM (n = 5, ordinary one-way ANOVA, followed by Tukey post-hoc test. ** $P < 0.01$). M: Schematic representation of marker expression for neural progenitors and cortical neurons by RT-PCR. Data are shown as mean±SEM (n ≧ 3 for each group, ordinary one-way ANOVA, followed by Tukey post-hoc test. * $P < 0.05$).

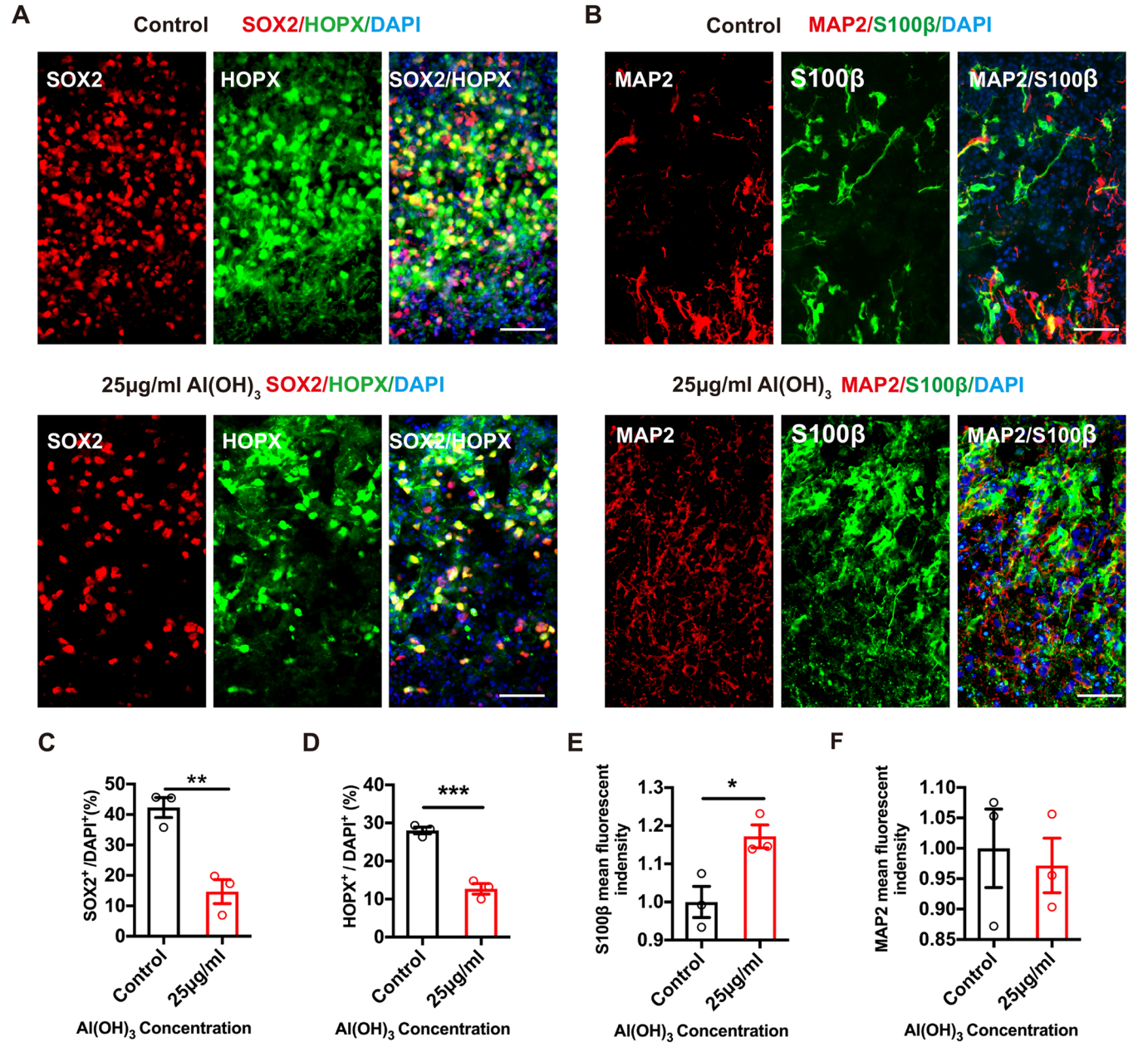

Fig. 8. Effects of 25 μg/ml $Al(OH)_3$ treatment on the oRG and astrocyte production in the day96-old cerebral organoids. A: Immunostaining for SOX2(red), oRG marker HOPX(green), and DAPI(blue) in the day96-old cerebral organoids after 6 days of treatment with $Al(OH)_3$ (0 and 25 μg/ml). Scale bars, 50 μm. B: Immunostaining for astrocyte marker S100β(green), neural marker MAP2(red), and DAPI(blue) in the day96-old cerebral organoids after six days of treatment with Al $(OH)_3$ (0 and 25 μg/ml). Scale bars, 50 μm. C,D: Qualification of $SOX2^+$ and $HOPX^+$ cells to $DAPI^+$ cells in the oSVZ of control and 25 μg/ml $Al(OH)_3$ treated cerebral organoids. E, F: Quantification of the relative mean fluorescent intensity of S100β and MAP2 in the cerebral organoids of treatment with $Al(OH)_3$ (0 and 25 μg/ml). Data are shown as mean±SEM. (n = 3, t test. ** $P < 0.01$).

CRediT authorship contribution statement

Liuyongwei Wang: Conceptualization, Methodology, Validation, Formal analysis, Investigation, Writing – original draft, Visualization. **Linqiang Mei:** Methodology, Investigation. **Zhenle Zang:** Methodology, Investigation. **Yun Cai:** Investigation. **Peiyan Jiang:** Methodology. **Lianyu Zhou:** Software. **Zhulin Du:** Software. **Ling Yang:** Methodology. **Zhanjun Gu:** Methodology. **Tianyao Liu:** Conceptualization, Supervision, Investigation, Writing – original draft, Formal analysis, Writing – review & editing. **Xiaotang Fan:** Conceptualization, Supervision, Project administration, Funding acquisition, Writing – review & editing.

Declaration of Competing Interest

The authors declare that they have no known competing financial interests or personal relationships that could have appeared to influence the work reported in this paper.

Data availability

Data will be made available on request.

Acknowledgments

This study was supported by the National Key R&D Program of China (2021YFA1101203), and the National Natural Science Foundation of China (No. 82071544).

Appendix A. Supplementary material

Supplementary data associated with this article can be found in the online version at doi:10.1016/j.ecoenv.2023.114863.

References

Alasfar, R.H., Isaifan, R.J., 2021. Aluminum environmental pollution: the silent killer. Environ. Sci. Pollut. Res. Int. 28, 44587–44597. https://doi.org/10.1007/s11356-021-14700-0.

Angrand, L., Masson, J.D., Rubio-Casillas, A., Nosten-Bertrand, M., Crepeaux, G., 2022. Inflammation and autophagy: a convergent point between autism spectrum disorder (ASD)-related genetic and environmental factors: focus on aluminum adjuvants. Toxics 10. https://doi.org/10.3390/toxics10090518.

Aziz, S., Ahmed, S., Karim, S.A., Tayyab, S., Shirazi, A., 2017. Toxic metals in maternal blood, cord blood and meconium of newborn infants in Pakistan. East Mediterr. Health J. 23, 678–687. https://doi.org/10.26719/2017.23.10.678.

Bershteyn, M., Nowakowski, T.J., Pollen, A.A., Di Lullo, E., Nene, A., Wynshaw-Boris, A., Kriegstein, A.R., 2017. Human iPSC-derived cerebral organoids model cellular features of lissencephaly and reveal prolonged mitosis of outer radial glia, 435-449 e434 Cell Stem Cell 20. https://doi.org/10.1016/j.stem.2016.12.007.

Bishop, N.J., Morley, R., Day, J.P., Lucas, A., 1997. Aluminum neurotoxicity in preterm infants receiving intravenous-feeding solutions. N. Engl. J. Med. 336, 1557–1561. https://doi.org/10.1056/NEJM199705293362203.

Bondy, S.C., 2010. The neurotoxicity of environmental aluminum is still an issue. Neurotoxicology 31, 575–581. https://doi.org/10.1016/j.neuro.2010.05.009.

Boretti, A., 2021. Reviewing the association between aluminum adjuvants in the vaccines and autism spectrum disorder. J. Trace Elem. Med. Biol. 66, 126764 https://doi.org/10.1016/j.jtemb.2021.126764.

Brunner, R., Jensen-Jarolim, E., Pali-Scholl, I., 2010. The ABC of clinical and experimental adjuvants–a brief overview. Immunol. Lett. 128, 29–35. https://doi.org/10.1016/j.imlet.2009.10.005.

Couette, M., Boisse, M.F., Maison, P., Brugieres, P., Cesaro, P., Chevalier, X., Gherardi, R. K., Bachoud-Levi, A.C., Authier, F.J., 2009. Long-term persistence of vaccine-derived aluminum hydroxide is associated with chronic cognitive dysfunction. J. Inorg. Biochem. 103, 1571–1578. https://doi.org/10.1016/j.jinorgbio.2009.08.005.

Dong, J., Feldmann, G., Huang, J., Wu, S., Zhang, N., Comerford, S.A., Gayyed, M.F., Anders, R.A., Maitra, A., Pan, D., 2007. Elucidation of a universal size-control mechanism in Drosophila and mammals. Cell 130, 1120–1133.

Exley, C., 2003. A biogeochemical cycle for aluminium? J. Inorg. Biochem. 97, 1–7. https://doi.org/10.1016/s0162-0134(03)00274-5.

Exley, C., 2013. Human exposure to aluminium. Environ. Sci. Process Impacts 15, 1807–1816. https://doi.org/10.1039/c3em00374d.

Fan, P., Wang, Y., Xu, M., Han, X., Liu, Y., 2022. The application of brain organoids in assessing neural toxicity. Front. Mol. Neurosci. 15, 799397 https://doi.org/10.3389/fnmol.2022.799397.

Gherardi, R.K., Eidi, H., Crépeaux, G., Authier, F.J., Cadusseau, J., 2015. Biopersistence and brain translocation of aluminum adjuvants of vaccines. Front. Neurol. 6, 4. https://doi.org/10.3389/fneur.2015.00004.

Giandomenico, S.L., Sutcliffe, M., Lancaster, M.A., 2021. Generation and long-term culture of advanced cerebral organoids for studying later stages of neural development. Nat. Protoc. 16, 579–602. https://doi.org/10.1038/s41596-020-00433-w.

Hamza Fares, B., Abdul Hussain Al-Tememy, H., Mohammed Baqir Al-Dhalimy, A., 2022. Evaluation of the toxic effects of aluminum hydroxide nanoparticles as adjuvants in vaccinated neonatal mice. Arch. Razi Inst. 77 (1), 221–228. https://doi.org/10.22092/ARI.2021.356418.1839.

Huang, J., Wu, S., Barrera, J., Matthews, K., Pan, D., 2005. The Hippo signaling pathway coordinately regulates cell proliferation and apoptosis by inactivating Yorkie, the Drosophila Homolog of YAP. Cell 122, 421–434.

Inohana, M., Eguchi, A., Nakamura, M., Nagahara, R., Onda, N., Nakajima, K., Saegusa, Y., Yoshida, T., Shibutani, M., 2018. Developmental exposure to aluminum chloride irreversibly affects postnatal hippocampal neurogenesis involving multiple functions in mice. Toxicol. Sci. 164, 264–277. https://doi.org/10.1093/toxsci/kfy081.

Jabali, A., Hoffrichter, A., Uzquiano, A., Marsoner, F., Wilkens, R., Siekmann, M., Bohl, B., Rossetti, A.C., Horschitz, S., Koch, P., Francis, F., Ladewig, J., 2022. Human cerebral organoids reveal progenitor pathology in EML1-linked cortical malformation. EMBO Rep. 23, e54027 https://doi.org/10.15252/embr.202154027.

Lancaster, M.A., Knoblich, J.A., 2014. Generation of cerebral organoids from human pluripotent stem cells. Nat. Protoc. 9, 2329–2340. https://doi.org/10.1038/nprot.2014.158.

Lancaster, M.A., Renner, M., Martin, C.A., Wenzel, D., Bicknell, L.S., Hurles, M.E., Homfray, T., Penninger, J.M., Jackson, A.P., Knoblich, J.A., 2013. Cerebral organoids model human brain development and microcephaly. Nature 501, 373–379. https://doi.org/10.1038/nature12517.

Lavado, A., Gangwar, R., Pare, J., Wan, S., Fan, Y., Cao, X., 2021a. YAP/TAZ maintain the proliferative capacity and structural organization of radial glial cells during brain development. Dev. Biol. 480, 39–49. https://doi.org/10.1016/j.ydbio.2021.08.010.

Lavado, A., Gangwar, R., Paré, J., Wan, S., Fan, Y., Cao, X.J.D.B., 2021b. YAP/TAZ Maintain the Proliferative Capacity and Structural Organization of Radial Glial Cells during Brain Development, 480, pp. 39–49.

Li, B., Xia, M., Zorec, R., Parpura, V., Verkhratsky, A., 2021. Astrocytes in heavy metal neurotoxicity and neurodegeneration. Brain Res. 1752, 147234 https://doi.org/10.1016/j.brainres.2020.147234.

Li, M., Gong, J., Gao, L., Zou, T., Kang, J., Xu, H., 2022. Advanced human developmental toxicity and teratogenicity assessment using human organoid models. Ecotoxicol. Environ. Saf. 235, 113429 https://doi.org/10.1016/j.ecoenv.2022.113429.

Li, R., Sun, L., Fang, A., Li, P., Wu, Q., Wang, X., 2017. Recapitulating cortical development with organoid culture in vitro and modeling abnormal spindle-like (ASPM related primary) microcephaly disease. Protein Cell 8, 823–833. https://doi.org/10.1007/s13238-017-0479-2.

Li, X., Aldayel, A.M., Cui, Z., 2014. Aluminum hydroxide nanoparticles show a stronger vaccine adjuvant activity than traditional aluminum hydroxide microparticles. J. Control. Release 173, 148–157. https://doi.org/10.1016/j.jconrel.2013.10.032.

Lindblad, E.B., 2004. Aluminium compounds for use in vaccines. Immunol. Cell Biol. 82, 497–505. https://doi.org/10.1111/j.0818-9641.2004.01286.x.

Liu, T., Ma, Y., Zhang, R., Zhong, H., Wang, L., Zhao, J., Yang, L., Fan, X., 2019. Resveratrol ameliorates estrogen deficiency-induced depression- and anxiety-like behaviors and hippocampal inflammation in mice. Psychopharmacology 236, 1385–1399. https://doi.org/10.1007/s00213-018-5148-5.

Lodge, E.J., Santambrogio, A., Russell, J.P., Xekouki, P., Jacques, T.S., Johnson, R.L., Thavaraj, S., Bornstein, S.R., Andoniadou, C.L., 2019. Homeostatic and tumourigenic activity of SOX2+ pituitary stem cells is controlled by the LATS/YAP/TAZ cascade. eLife 8. https://doi.org/10.7554/eLife.43996.

Lujan, L., Perez, M., Salazar, E., Alvarez, N., Gimeno, M., Pinczowski, P., Irusta, S., Santamaria, J., Insausti, N., Cortes, Y., Figueras, L., Cuartielles, I., Vila, M., Fantova, E., Chapulle, J.L., 2013. Autoimmune/autoinflammatory syndrome induced by adjuvants (ASIA syndrome) in commercial sheep. Immunol. Res. 56, 317–324. https://doi.org/10.1007/s12026-013-8404-0.

Mariani, J., Coppola, G., Zhang, P., Abyzov, A., Provini, L., Tomasini, L., Amenduni, M., Szekely, A., Palejev, D., Wilson, M., Gerstein, M., Grigorenko, E.L., Chawarska, K., Pelphrey, K.A., Howe, J.R., Vaccarino, F.M., 2015. FOXG1-dependent dysregulation of GABA/glutamate neuron differentiation in autism spectrum disorders. Cell 162, 375–390. https://doi.org/10.1016/j.cell.2015.06.034.

Mold, M., Linhart, C., Gomez-Ramirez, J., Villegas-Lanau, A., Exley, C., 2020. Aluminum and amyloid-beta in familial Alzheimer's disease. J. Alzheimers Dis. 73, 1627–1635. https://doi.org/10.3233/JAD-191140.

Niu, Q., 2018. Overview of the RElationship between Aluminum Exposure and Health of Human Being. Adv. Exp. Med. Biol. 1091, 1–31. https://doi.org/10.1007/978-981-13-1370-7_1.

Petrik, M.S., Wong, M.C., Tabata, R.C., Garry, R.F., Shaw, C.A., 2007. Aluminum adjuvant linked to Gulf War illness induces motor neuron death in mice. Neuromol. Med. 9, 83–100. https://doi.org/10.1385/nmm:9:1:83.

Pogue, A.I., Lukiw, W.J., 2016. Aluminum, the genetic apparatus of the human CNS and Alzheimer's disease (AD). Morphologie 100, 56–64. https://doi.org/10.1016/j.morpho.2016.01.001.

Principi, N., Esposito, S., 2018. Aluminum in vaccines: does it create a safety problem? Vaccine 36, 5825–5831. https://doi.org/10.1016/j.vaccine.2018.08.036.

Qian, X., Song, H., Ming, G.L., 2019. Brain organoids: advances, applications and challenges. Development 146. https://doi.org/10.1242/dev.166074.

Ramos, A., Camargo, F.D., 2012. The Hippo signaling pathway and stem cell biology. Trends Cell Biol. 22, 339–346. https://doi.org/10.1016/j.tcb.2012.04.006.
Reichert, K.P., Schetinger, M.R.C., Pillat, M.M., Bottari, N.B., Palma, T.V., Gutierres, J. M., Ulrich, H., Andrade, C.M., Exley, C., Morsch, V.M.M., 2019. Aluminum affects neural phenotype determination of embryonic neural progenitor cells. Arch. Toxicol. 93, 2515–2524. https://doi.org/10.1007/s00204-019-02522-6.
Reuven, N., Adler, J., Meltser, V., Shaul, Y., 2013. The Hippo pathway kinase Lats2 prevents DNA damage-induced apoptosis through inhibition of the tyrosine kinase c-Abl. Cell Death Differ. 20, 1330–1340. https://doi.org/10.1038/cdd.2013.83.
Shaw, C.A., 2018. Aluminum as a CNS and immune system toxin across the life span. Adv. Exp. Med. Biol. 1091, 53–83. https://doi.org/10.1007/978-981-13-1370-7_4.
Shaw, C.A., Tomljenovic, L., 2013. Aluminum in the central nervous system (CNS): toxicity in humans and animals, vaccine adjuvants, and autoimmunity. Immunol. Res. 56, 304–316. https://doi.org/10.1007/s12026-013-8403-1.
Sheth, S.K.S., Li, Y., Shaw, C.A., 2018. Is exposure to aluminium adjuvants associated with social impairments in mice? A pilot study. J. Inorg. Biochem. 181, 96–103. https://doi.org/10.1016/j.jinorgbio.2017.11.012.
Shikata, Y., Okada, T., Hashimoto, M., Ellis, T., Matsumaru, D., Shiroishi, T., Ogawa, M., Wainwright, B., Motoyama, J., 2011. Ptch1-mediated dosage-dependent action of Shh signaling regulates neural progenitor development at late gestational stages. Dev. Biol. 349, 147–159. https://doi.org/10.1016/j.ydbio.2010.10.014.
Terry, B.K., Kim, S., 2022. The Role of Hippo-YAP/TAZ Signaling in Brain Development, 251, pp. 1644–1665. ⟨https://doi.org/10.1002/dvdy.504⟩.
Tomljenovic, L., Shaw, C.A., 2011. Do aluminum vaccine adjuvants contribute to the rising prevalence of autism? J. Inorg. Biochem. 105, 1489–1499. https://doi.org/10.1016/j.jinorgbio.2011.08.008.
Walton, J.R., 2007. A longitudinal study of rats chronically exposed to aluminum at human dietary levels. Neurosci. Lett. 412, 29–33. https://doi.org/10.1016/j.neulet.2006.08.093.
Wang, L., 2018. Entry and deposit of aluminum in the brain. Adv. Exp. Med. Biol. 1091, 39–51. https://doi.org/10.1007/978-981-13-1370-7_3.
Yokel, R.A., Hicks, C.L., Florence, R.L., 2008. Aluminum bioavailability from basic sodium aluminum phosphate, an approved food additive emulsifying agent, incorporated in cheese. Food Chem. Toxicol. 46, 2261–2266. https://doi.org/10.1016/j.fct.2008.03.004.
Zhang, H., 2018. Aluminum-induced electrophysiological variation, synaptic plasticity impairment, and related mechanism. Adv. Exp. Med. Biol. 1091, 161–172. https://doi.org/10.1007/978-981-13-1370-7_9.
Zhao, N., Zhou, L., Lu, Q., Wang, S., Sun, Y., Ding, Y., Liu, M., He, H., Lang, T., 2022. SOX2 maintains the stemness of retinoblastoma stem-like cells through Hippo/YAP signaling pathway. Exp. Eye Res. 214, 108887 https://doi.org/10.1016/j.exer.2021.108887.